nature communications

Article

https://doi.org/10.1038/s41467-024-50859-z

The coupling of rotational and translational dynamics for rapid diffusion of nanorods in macromolecular networks

Received: 23 February 2024

Accepted: 23 July 2024

Binghui Xue[1], **Yuan Liu**[1], **Ye Tian**[2] & **Panchao Yin**[1]

The rod-like viruses show anomalously rapid diffusion in bio-tissue networks originated from the rotation-facilitated transportation; however, the experimental investigation of the correlation of the rotational and translational dynamics is still in blank. Herein, typical rod-like and spherical gold nanoparticles (NPs) are dispersed in the classical Tetra-PEG gels, respectively, as model systems for light scattering studies. The contributions from translational and rotational diffusive dynamics, and network fluctuation dynamics can be well-resolved and the stretch exponent of rotational dynamics at 0.25 is proven to be the fingerprint for the coupled rotational and translational dynamics of nanorods. The rotation facilitated re-orientation finally leads to the fast transportation of nanorods. The discoveries are confirmed to be valid for rod-like biomacromolecule systems by studying the diffusive dynamics of Tobacco mosaic virus in gels. The work can be inspiring for the development of protocols to prevent infection of microorganism and regulate the transportation of nano-medicines.

The transportation of biological and artificial nanoparticles (NPs) in various tissues represents the critical process for the infection of microorganisms and the targeted delivery of nano-medicines and diagnostic probes[1–4]. Generally, the underlying physics can be described as the diffusion of NPs confined in networks with different viscoelasticity. Interestingly, in comparison to isotropic NPs, the nanorods show anomalously rapid diffusion in networks from theoretical studies[5,6]. Experimentally, the rod-like biomacromolecules and micro-organisms are observed to possess high mobility in tissues[1,7–10]. The Stokes-Einstein relation is invalid to describe the dynamics of nanorods due to the breakdown of continuum model[11]. The increased mobility of nanorods has been attributed to the additional freedom degrees of rotation, while the rotational dynamics allow nanorods to enter adjacent mesh more easily compared to isotropic NPs with similar sizes[7,12]. In previous research, Jain et al. reported the faster tumor penetration speed of rod-like NPs in comparison to spherical NPs by using the multiphoton microscopy technique[1]. Gao et al. observed a similar phenomenon in stimulated emission of depletion microscopy studies, and further simulation was applied to confirm the enhancement of translational diffusion by rotational dynamics[7]. Yan et al. focused on the fast sliding dynamics of thick rod in a network both in experiment and simulation and revealed the physical origin based on the calculation of the free energy landscape[13]. Composto et al. applied single particle tracking to study the rod dynamics during the gelation process and elucidated the potential mechanisms for the caging to mobile behavior of nanorods[8]. The non-Gaussian displacement distributions of nanorods is also uncovered, which is in consistence with the results obtained by Conrad et al.[14]. Although the explanations inferred yet are reasonable, the quantitative relationship between rotational and translational dynamics and their correlation with nanorod size and network mesh size still hides in the mist.

Quasi-elastic scattering can be applied to probe relaxation dynamics of soft matter at selected spatiotemporal ranges, and the measurements contain both information on relaxation time and the

---

[1] State Key Laboratory of Luminescent Materials and Devices & South China Advanced Institute for Soft Matter Science and Technology, Guangdong Basic Research Center of Excellence for Energy & Information Polymer Materials, South China University of Technology, Guangzhou, China. [2] Key Laboratory of Photochemical Conversion and Optoelectronic Materials, Technical Institute of Physics and Chemistry, Chinese Academy of Sciences, Beijing, P.R. China.
e-mail: yinpc@scut.edu.cn

corresponding spatial scale for certain relaxation processes[15–17]. When the spatio-temporal window is broad enough, the contribution of hierarchical relaxation processes can be quantitatively determined, and their structural origin can be ascribed[18]. Moreover, due to their sensitivity to the rotation motion of anisotropic particles, the depolarized mode of quasi-elastic scattering can be used to separately measure rotational relaxation dynamics[19–21]. Herein, depolarized dynamic light scattering (DDLS) together with dynamic light scattering (DLS) is applied to study the relaxation dynamics of rod and spherical gold nanoparticles (NPs) confined in classical tetra-poly (ethylene glycol) (tetra-PEG) hydrogel. For anisotropic particles, the off-diagonal elements of the polarizability tensor are not zero, which leads to the changing of the polarization. Therefore, optically anisotropic particles will contribute a signal of depolarized scattering, and the orientational correlation function can be measurable[19]. As a result, the translational and rotational dynamics are quantitively and separately determined, and the correlation can be deciphered. With rigorous correction of the intrinsic nonergodicity of hydrogel system, we report a rotation reorientation induced translation dynamical behavior of nanorod whose translation is highly coupled with its rotation process, and the same behavior can also be extended to biological systems, e.g., tobacco mosaic virus (TMV).

Results

Hydrogel characterization

The mesh size ξ of the host hydrogel is measured using ensemble-averaged static light scattering intensity ($\langle I(q)\rangle_E$) upon the fitting using the Ornstein-Zernike equation[15,22,23]. As shown in Supplementary Fig. 1 (a), a plot of $1/\langle I(q)\rangle_E$ versus q^2 is linear, and the respective mesh size is 20 nm, and this mesh size is also consistent with the results of rheology (Supplementary Fig. 2a, b, and Supplementary Note 3). The scattering intensity at different sub-ensembles is consistent, verifying the near-perfect homogeneity of the selected model gel system (Supplementary Fig. 3a). For the pure host gel, two relaxation modes can be observed in DLS measurements (Supplementary Fig. 1b), and the dominant mode contributes about 93% of the correlation function, whose decay rate is proportional to q^2 (Supplementary Fig. 1c) with a diffusion coefficient of $D_{gel} = (5.44 \pm 0.13) \times 10^{-11}\, m^2/s$. For gels, the electric field correlation function $g_1(q,t)$ is proportional to the correlation function of the longitudinal displacement $\mu_l(q,t)$ of strands, as expressed:

$$g_1(q,t) \sim <\mu_l(q,0)\mu_l(q,t)> = <\mu_l^2(q,0)> e^{-\Gamma t}, \Gamma = D_{gel}q^2 \qquad (1)$$

where $D_{gel} = \frac{M_l}{f}$ (M_l is the longitudinal modulus of the gel, f is the friction coefficient). D_{gel} is related to the gel elasticity as it is proportional to the longitudinal modulus of gel[24].

As shown in Supplementary Fig. 1d, the decay rate of the other mode is not linear with q^2, which represents non-diffusive dynamics[25,26]. The minor mode is related to the tiny amount of unavoidable chemical inhomogeneities, and it has negligible effect on the following studies of NP diffusive dynamics since the ratio is low. The homogeneity has also been verified by scattering intensity at different sub-ensembles (Supplementary Fig. 3a)[27].

Dynamics of gold nanorods in hydrogels

We have studied two gold nanorods named NR50 and NR85 with sizes 50 nm * 20 nm and 85 nm * 17 nm, respectively, and the size of TMV used is 300 nm * 18 nm, while the gold nanosphere named NS32 has a diameter of 32 nm. These particles are loaded within the gels without affecting the structure of networks or exhibiting strong interaction with gel strands, as supported by the rheology results (Supplementary Fig. 2). The structure parameters of these particles have been confirmed from small angle X-ray scattering (SAXS) (Supplementary Fig. 3b–e), DLS studies (Supplementary Table 1) and TEM (transmission electron microscopy) (Supplementary Fig. 4). The normalized first-order correlation function $g_{1,F,VH}(q,t)$ s of DDLS of NR50 in hydrogel matrix at different Qs together with the fittings are shown in Fig. 1a, and the respective best-fitting function can be expressed as a sum of two exponential decays and a stretched exponential decay:

$$g_{1,F,VH}(q,t) = A_1 \exp(-\Gamma_1 t) + A_2 \exp(-\Gamma_2 t) + (1 - A_1 - A_2)\exp(-(\Gamma_s t)^\beta) \qquad (2)$$

where Γ is the decay rate, A is the weighting factor, and β is the stretched exponent. The linear fitting of the obtained decay rate on Q affords the translational and rotational diffusion coefficients from the slope and intercept respectively. As shown in Fig. 1b, the Q dependence of the decay rate of the first mode (Γ_1) of NR50 exhibits a slope of zero, suggesting the absence of the translational motion of the particles. The first mode Γ_1 can be attributed to the locally partial rotation of the nanorod within meshes since the D_r is identical to that of the nanorod in water after viscosity correction. The apparent $D_r\,(7194\ s^{-1})$ in gels is about 25% of $D_r\,(27874\ s^{-1})$ of nanorods in water, while the viscosity of tetra-PEG solution with the same concentration as the hydrogel matrix is about four times of pure water (Supplementary Fig. 3f). Similarly, the second mode Γ_2 between Γ_1 and Γ_s, only exports a rotational diffusion coefficient of 381 s^{-1} without obvious translational contributions, and we consider this mode as another local rotation process. The stretched mode Γ_s is actually an anomalous rotation process since its deviation from exponential decay[28], and the averaged β at different angles (Supplementary Fig. 5a) is:

$$\beta = 0.24 \pm 0.02$$

The stretched exponential decay represents a distribution of relaxation times of rods taking different positions and orientations inside the gel meshes, whereas the elastic deformation energy of gel strands confining a nanorod varies depending on the specific orientations of the rods. The thermal fluctuation could possibly drive the rotation of the rod to achieve the hopping of rod orientation, which finally results in the rotational diffusion within adjacent meshes. The rotational mode of a re-orientation process can contribute to the translational diffusion of rods, and the translation is highly coupled to the rotation.

Theoretical analysis regarding the rotation process is also conducted for the deep interpretation of experimental results. The rotation and translation of the rod will be confined once the rod length is larger than the network mesh size and therefore, the confined rods can have different orientations within meshes (Fig. 1e–h)[12]. Each orientation corresponds to a certain possible rotatable angle ψ, which is of order:

$$\psi \sim \frac{\xi}{l}\frac{\xi}{d} \qquad (3)$$

where d is the rod diameter, ξ, and l is the length of rod inside the gel meshes. As shown in Fig. 1e–h, the rod is sliced by several meshes, and the meshes are disturbed and stretched by the rod. The parameter l is used to describe the length of the subregions of rods inside one gel mesh. Here, $\frac{\xi}{l}$ is the Taylor expansion of $\arcsin(\frac{\xi}{l})$, which is the main part of the description of the rotatable angle. However, the above term holds assuming a very small diameter, which is not valid in our system, and a correction term $\frac{\xi}{d}$ is introduced as the rotatable angle becomes smaller for a larger diameter. Here, the parameter ψ doesn't equal to the practical value of the rotatable angle but only plays as a scaling argument for the measure of the rotatable extent of the rod. Therefore, the confinement free energy, F_{conf}, of the strands can be derived by considering the elastic deformation energy of gel strands under the

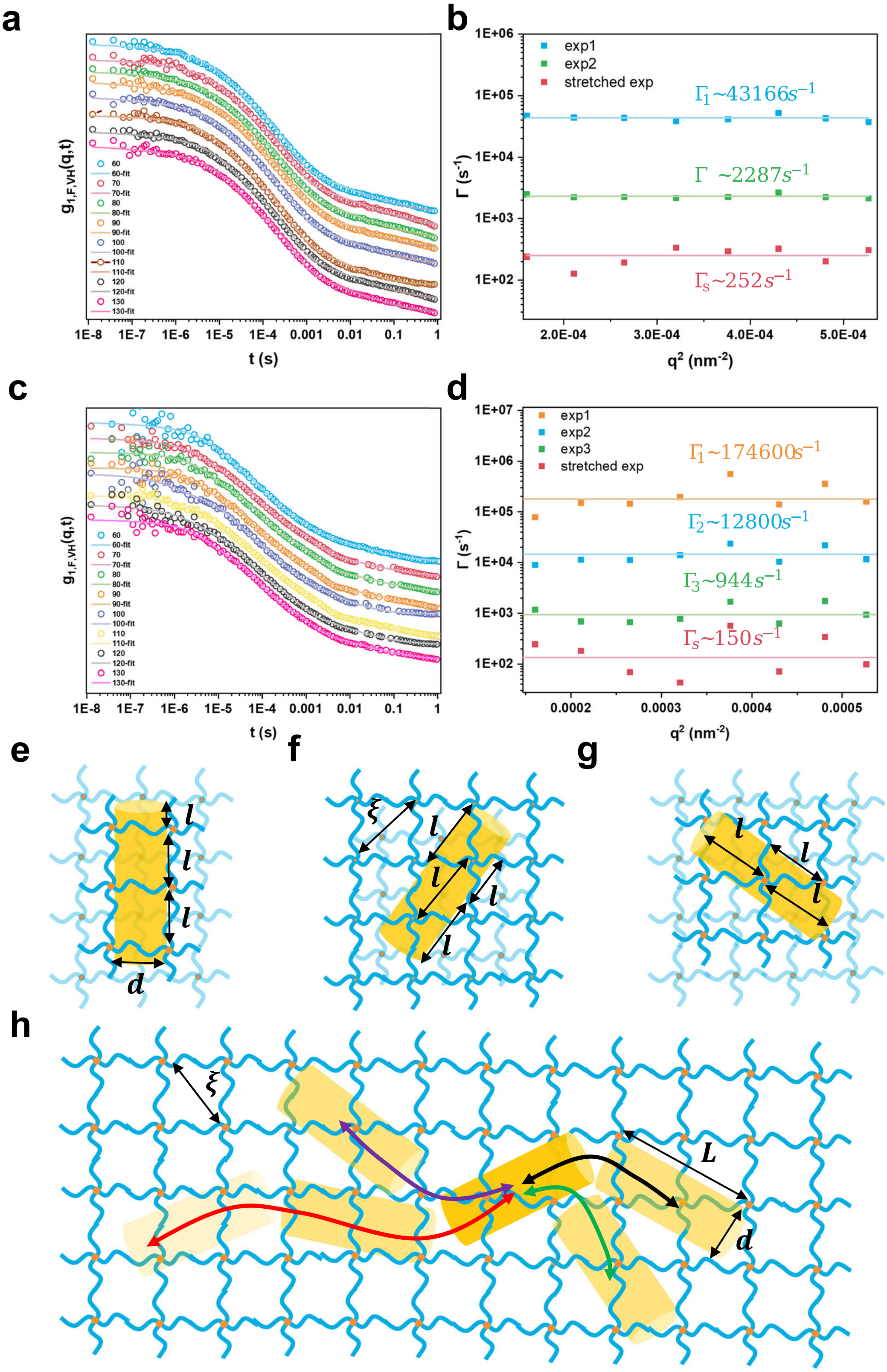

Fig. 1 | Dynamics of NR50 and NR85 in TPEG gels and schematics illustrating the physical picture. **a** The fluctuation part of the ensemble-averaged correlation function of NR50 inside hydrogel together with the best-fitting curve. **b** q^2 dependence of the three relaxation rates of NR50 measured in DDLS. **c** The fluctuation part of the ensemble-averaged correlation function of NR85 inside hydrogel together with the best-fitting curve. **d** The four relaxation rates of NR85 measured in DDLS as a function of q^2. **e**–**g** Schematics of rods taking different orientations within gel meshes when their rotations are strongly confined. **h** Schematics of the translational motion induced or assisted by the rotation re-orientation process, the translational motion is random, and the possible back-and-forth motion is indicated by the double arrow label. The schematics shown in e-h are illustrated by taking the NR50-TPEG system as an example.

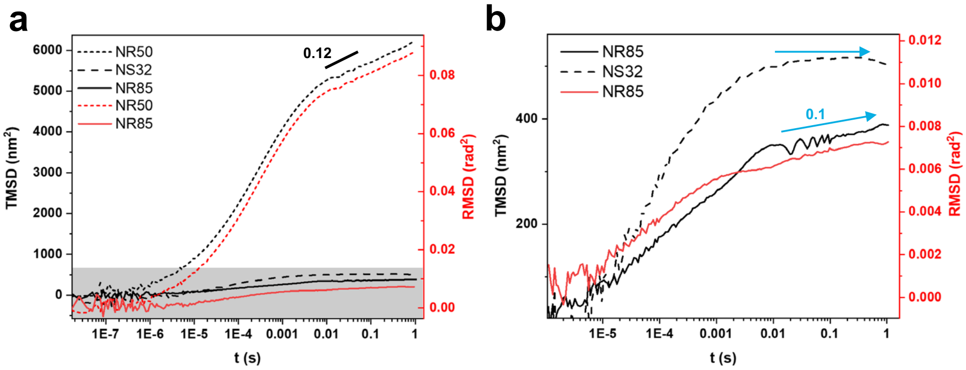

Fig. 2 | The TMSD and RMSD of the particles studied. a TMSD of NR50, NR85, NS32, and RMSD of NR50, NR85. **b** Enlarged gray part of (**a**).

interference of the confined rods with specific orientation[29,30] (Supplementary Note 1):

$$F_{conf} \sim A_l k_B T l \tag{4}$$

where A_l is the pre-factor ($A_l \sim \frac{1}{\xi}$), k_B is the Boltzmann constant and T is the absolute temperature. The corresponding probability of the existence of a specific orientation can be described by the Gibbs distribution function as[31]:

$$P(\psi) \sim \exp\left(-\frac{F_{conf}}{k_B T}\right) \sim \exp(-A_l l) \tag{5}$$

The rotation process is actually a re-orientation process during a short time interval (Δt), and the relaxation rate is

$$6D_r = \Gamma \sim \frac{\psi^2}{\Delta t} \sim \frac{\xi^4}{d^2 l^2 \Delta t} \tag{6}$$

the corresponding displacement during Δt is in connection with ξ as we assume that the re-orientation induces the entrance into adjacent meshes, and such consideration is reasonable as suggested from the similar trend of TMSD (translational mean-square displacements) and RMSD (rotational mean-square displacements) of rods (Fig. 2). The time interval follows $\Delta t \sim \frac{\xi^2 \eta_{local} l}{k_B T}$ based on the diffusion equation consideration[32], where the η_{local} is the local viscosity as the rod doesn't experience the bulk viscosity, and the expression for D_r covers the contribution from the parameter of d and ξ. Then, the relaxation rate can be expressed as:

$$D_r \sim \Gamma \sim \frac{k_B T \xi^2}{d^2 \eta_{local} l^3} \sim l^{-3} \tag{7}$$

The experimentally measured $g_1(t)$ is the superposition of rods taking different orientations considering their respective probability ($P(\psi) \sim P(l)$):

$$g_1(t) \sim \int_0^L P(l)\exp(-\Gamma t)dl \sim \int_0^{+\infty} P(l)\exp(-\Gamma t)dl \tag{8}$$

Substituting Eqs. (5) and (7) into Eq. (8), and computing the integral via saddle point approximation (Supplementary Note 2) considering the feature of fast decay of exponential function, we get the expression[25,33]:

$$g_1(t) \sim \exp(-(\Gamma t)^{\frac{1}{4}}) \tag{9}$$

The obtained stretched exponential decay originating from the linear superposition of relaxations with different characteristic times is different from the ordinary exponential decay suggested by the Stokes-Einstein-Debye relation. As a result, the proposed rotation dynamics for the re-orientation of rods at different orientations in the gel meshes lead to the theoretical derivation of $\beta \approx \frac{1}{4}$, which is consistent with the above experimental observations. Actually, the exponent of 0.25 is directly related to the relaxation time distribution while such theoretical assumption can also be well verified by a recent MD simulation work by Yan et al.[12]. The performed integral considers not only the cooperative results of the subregions of one rod but also the rods with various orientations. It's actually the ensemble-averaged results that we measure in the scattering experiment. The coincidence confirms that the re-orientation process helps the fast translation of the rod within networks, as the re-orientation of the rod raises the probability of moving into other meshes (Fig. 1h). This should be a reliable explanation for the speculation about the rotation-facilitated translation of nanorods by previous work[7,8].

Compared to NR50, NR85 exhibits similar dynamical behaviors both in DLS and DDLS results, but an extra exponential decay is required to fulfill best-fitting (Fig. 1c, d). The extra dynamical mode with a ratio of 9% corresponds to the rotation coupled to network fluctuation, as the relaxation time ($\Gamma_1 \sim 174600\ s^{-1}$) is similar to the characteristic fluctuation time of the network ($\Gamma_{gel} = \frac{D_{gel}}{\xi^2} \sim 135000\ s^{-1}$). This extra rotation coupled to the network is due to the large rod length compared to the mesh size, and the coupling is weak. Considering the low ratio of coupling in the NR85 system, the coupling effect of NR50 may be too weak to be observed in our experiments. Apart from the extra rotation process, the other three dynamical modes are the same as NR50, and the characteristic rotation-induced translation dynamic still holds as the averaged exponent at different angles is $\beta = 0.27 \pm 0.015$ (Supplementary Fig. 5 (b)). This consistency of the obtained dynamics with theoretical analysis and the gel's intrinsic properties further verifies the credibility of the fitting function.

The coupling of translational and rotational diffusive dynamics

The diffusive dynamics of spherical NPs are studied as a control to understand the coupling of translational and rotational diffusive dynamics of nanorods, and NS32 is selected by considering that its translational diffusion coefficient is similar to NR85 and NR50 in water. As for nanospheres with a smaller size comparable to mesh size, free diffusion of nanosphere slower than the prediction of the Stokes-Einstein relation is observed, and the detailed analysis is shown in Supplementary Note 4. The DDLS and DLS studies of NS32 in gels give different results (Fig. 3a), where a mode at micro-seconds scale can be found absent in DDLS compared to DLS obviously. This absent mode is related to translational fluctuations, which are filtered out by the polarizer in DDLS[34]. The best fit for DLS can be accomplished by $g_{1,F,VV}(q,t) = A_1\exp(-\Gamma_1 t) + A_2\exp(-(\Gamma_{s1}t)^{\alpha}) + (1 - A_1 - A_2)\exp(-(\Gamma_{s2}t)^{\beta})$, while DDLS only needs two stretched

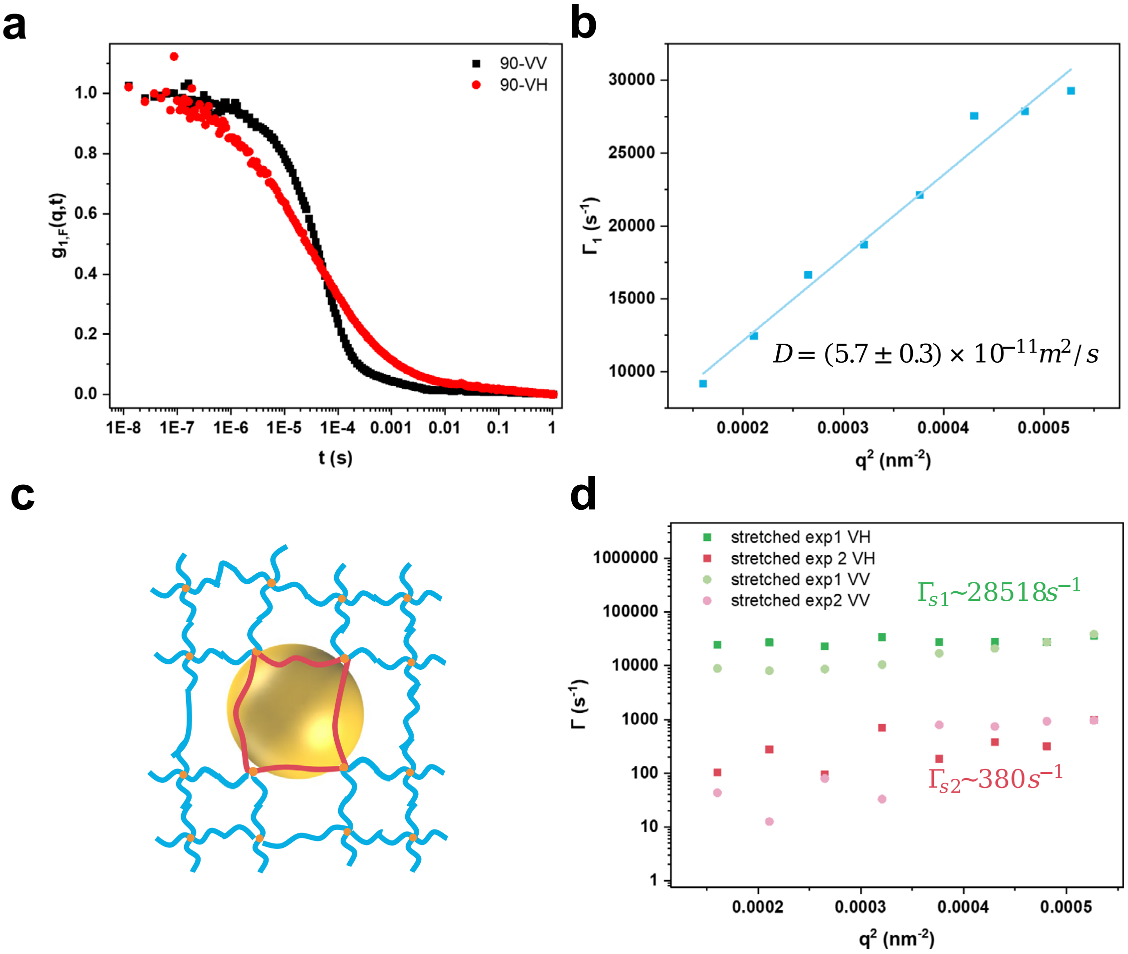

Fig. 3 | The dynamics of NS32 in TPEG gel and the schematic. a Correlation functions of DDLS and DLS of NS32 confined in hydrogel at a scattering angle of 90 degrees. **b** Fitting results of Γ versus q^2 of the first mode of DLS results. **c** Schematic of sphere trapped inside meshes of the hydrogel. **d** q^2 dependence of relaxation rates of the other two modes in DLS and the respective relaxation rates obtained from DDLS is also plotted.

exponential decays to fulfill the best fit in comparison to DLS, and these two modes correspond to rotational motions. Actually, the non-perfect surface of the nanosphere with relatively small sizes contributes to its anisotropy and the so-resulting signals of DDLS[35].

Regarding the relaxation dynamics of NS32, the first dynamical mode is diffusive since the angle dependence of Γ_1 follows $\Gamma = Dq^2$ (Fig. 3b). The diffusion coefficient obtained is $D = 5.7 \times 10^{-11}\ m^2/s$, which is even faster than the diffusion of the nanosphere in water (Supplementary Table 1). Therefore, this diffusive mode is definitely not the free diffusion of NS32 within gel networks. Actually, the diffusion coefficient is close to the intrinsic fluctuation dynamics of gels ($D_{gel} = 5.4 \times 10^{-11}\ m^2/s$). Therefore, the diffusive mode is highly coupled to the fluctuation of the hydrogel. The diameter of NS32 is about 1.5 times the network mesh size, and the sphere will be forced to fluctuate together with the network (Fig. 3c), and the mean squared displacement of NS32 will be immobilized within the mesh as shown in the plateau in Fig. 2b. In fact, similar observation is also reported, where gold nanospheres are used as tracers to monitor the gelation process, and the spheres exhibit a diffusion coefficient faster than in pure solvents[36]. The other two stretched exponential decays are from the rotation coupled to chain dynamics, and they are consistent in DLS and DDLS measurements (Fig. 3d). The stretched exponent α is close to 0.5 (Supplementary Fig. 5c), and the same phenomenon is always observed in polymer rubbery states[37]. The stretched exponent β is close to 0.4 (Supplementary Fig. 5c), which is consistent with the dynamical feature of Zimm dynamics originating from the crosslinked polymer networks[33]. In short, the NS32 is highly confined in gel mesh and its relaxation dynamics is on the same tune with the gel network, which is the same as the principle of nano-rheology[38–40].

Translational (TMSD, $\langle \delta r^2(t) \rangle$) and rotational mean-square (RMSD, $\langle \delta\theta^2(t) \rangle$) displacements are extracted from the correlation function of DDLS studies for direct comparison of the diffusive behavior of spherical NPs and nanorods. According to Eqs. (16) and (17) in methods part, we can obtain the TMSD and RMSD of the NPs confined in gels. As shown in Fig. 2a, the diffusion of NR50 is much faster than NR85 and NS32 within the hydrogel matrix, even if these three particles have similar diffusion coefficients in water (Supplementary Table 1). However, the dynamics of NR50 within the experimental time scale don't exhibit Brownian diffusion feature. We attribute the difference between NR85 and NR50 to the stronger confinement of gel on NR85, and that's also the reason for the observable weak coupling between NR85 and gel network (mode Γ_1 with a low ratio of 9%) (Fig. 1d). This difference doesn't affect the confirmation of the characteristic rotation re-orientation dynamics. Within the experimental scale, the diffusion of NR85 is slower than NS32, but the NR85 tends to move to broader space compared to NS32, as the TMSD of NS32 exhibits a plateau (Fig. 2b). Such plateau-like regime at the long time scale of NS32 is consistent with the fitting results, the dynamics of spherical NPs is on the same tune with gel networks due to the strong confinement effect. For NR85, the slope of 0.1 of TMSD at a long time scale represents the sub-diffusion feature, which is also consistent with the fitting analysis. It confirms that the characteristic rotation re-orientation dynamics do

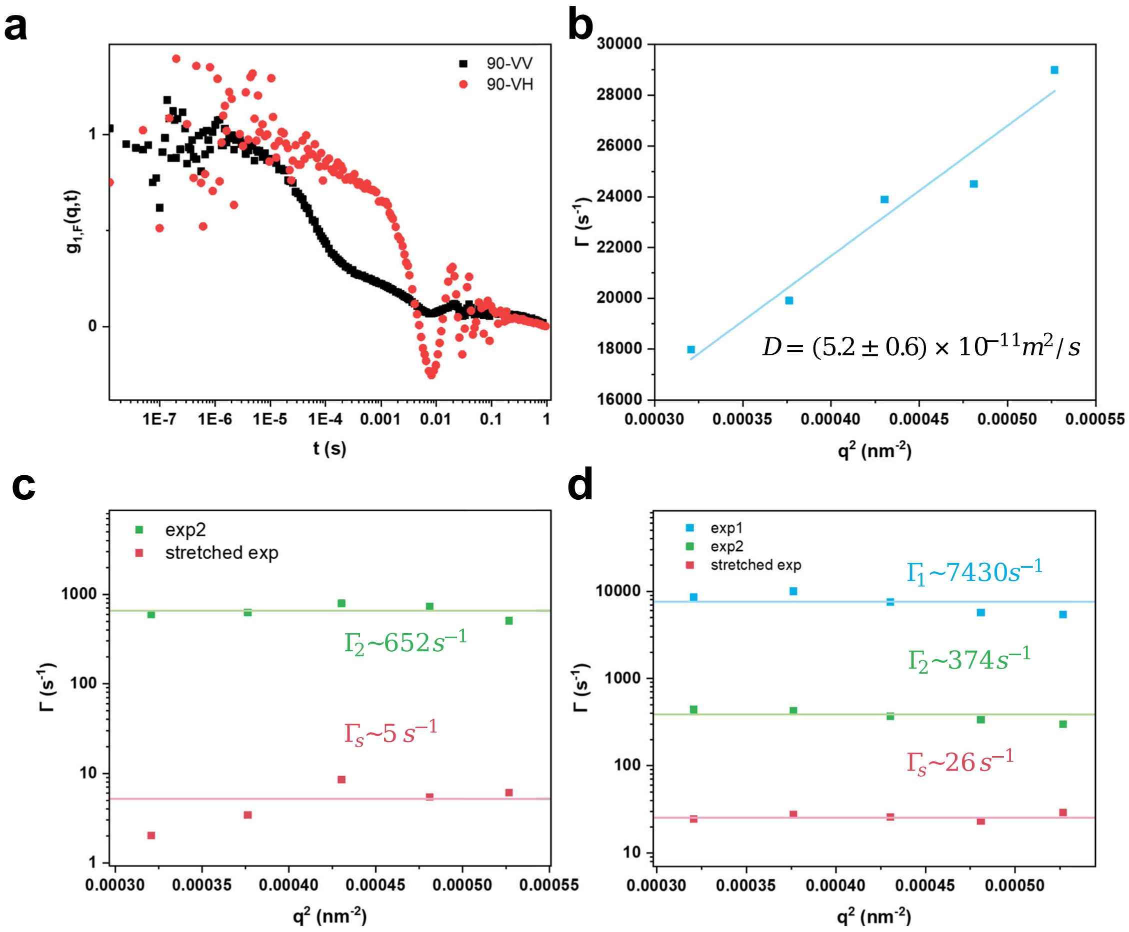

Fig. 4 | The dynamics of TMV in TPEG gel and PEGDA gel. a Correlation functions of DDLS and DLS of TMV confined in hydrogel at a scattering angle of 90 degrees (TMV-TPEG system). **b** DLS results: the linear fitting of the relaxation rate of the first mode versus q^2 (TMV-TPEG system). **c** q^2 dependence of relaxation rates of the other two relaxations obtained from DLS (TMV-TPEG system). **d** q^2 dependence of relaxation rates of the three relaxations of the TMV-PEGDA system.

contribute to the diffusion of rods. The same trend can be observed in RMSD and TMSD for both NR85 and NR50, especially at longer time scales, which further verifies the coupling between rotation and translation, and the translation induced by rotation re-orientation.

Extension to biological system

The understanding of the dynamics of nanorods is important for biomedical applications, and herein, rod-like biomacromolecule TMV, is studied in gels for their unique diffusive dynamics[41]. The dynamics of TMV in pure water were first analyzed as a control, the rotational and translational diffusion coefficients were obtained (Supplementary Table 1), which are the same as in previous literature. Once the TMV is confined in the gel network, the dynamics of TMV are severely restricted, as suggested by our light scattering experiments. The fastest relaxation mode observed in DLS is absent in DDLS, and the respective correlation functions are shown in Fig. 4a. The invisibility of this mode in DDLS demonstrates its translational nature. We consider this process as the motion of TMV coupled to the network fluctuation, as the fastest dynamical mode Γ_1 follows $\Gamma = Dq^2$ and the diffusion coefficient is $(5.2 \pm 0.6) \times 10^{-11}\ m^2/s$, which is close to the D_{gel} (Fig. 4b).

The significance of our studies on the rotation re-orientation process relies on the extension in biological systems, and we demonstrate its existence via the stretch exponent $\beta = 0.26 \pm 0.03$ of the stretched exponential decay (Supplementary Fig. 5d). However, the ratio of this process is just about 10%, which is much lower than in NR50 (~45%) and NR85 (~40%). Although the confinement is strong considering the large length, the dynamics of TMV are not completely frozen. It still exhibits the same fingerprint of coupled rotation and translation as observed in gold nanorod systems, even if the ratio is low. The other mode Γ_2 corresponds to rotation coupled to network fluctuation at a larger scale, since $\frac{D_{gel}}{L_{TMV}^2} = 600\ s^{-1}$, which is close to Γ_2 measured (Fig. 4c). In short, the other two relaxation process apart from the rotation re-orientation process are dynamics coupled to network fluctuation. To further study the strong confinement exerted on the TMV, the gel mesh sizes have been varied to study the confined dynamics of TMV systematically. A PEGDA hydrogel with mesh size ~40 nm is prepared with TMV loaded (Supplementary Fig. 6d and Supplementary Note 3, 5). The dynamics of TMV within the PEGDA gel are similar to NR50 and NR85, and the normalized first-order correlation function $g_{1,F,VH}(q,t)$ s of DDLS of TMV in PEGDA hydrogel at different Qs can be well fitted by a sum of two exponential decays and a stretched exponential decay (Supplementary Fig. 5e):

$$g_{1,F,VH}(q,t) = A_1 \exp(-\Gamma_1 t) + A_2 \exp(-\Gamma_2 t) + (1 - A_1 - A_2) \exp\left(-(\Gamma_s t)^{\beta}\right).$$

The decay rates of these three relaxations exhibit the same Q dependence of $\Gamma \sim q^0$ (Fig. 4d). Similar to NR85 and TMV in TPEG gels, the first mode Γ_1 corresponds to the rotation coupled to network fluctuation, since $\frac{D_{gel}}{(90nm)^2} \sim 7037\ s^{-1}$, and this length scale is smaller than the coupling scale of TMV in TPEG hydrogel while larger than the coupling scale of NR85. Taking the lengths of nanoparticles and mesh sizes into consideration, this phenomenon should originate from different extents of confinement.

The second mode Γ_2 is the locally partial rotation of TMV within meshes, as the D_r is the same that of TMV in water after viscosity correction. The apparent D_r $(62\,s^{-1})$ TMV in PEGDA gels is about 33% of D_r $(191\,s^{-1})$ of TMV in water, while the viscosity of PEGDA solution with the same concentration as the gel matrix is about three times of pure water (Supplementary Fig. 3f). The third mode of stretched exponential decay exhibits stretched exponent of $\beta = 0.26 \pm 0.011$ (Supplementary Fig. 5f), which demonstrates the existence of the characteristic rotation re-orientation process in TMV-PEGDA gel system. In comparison to TMV in TPEG gel, the ratio of such relaxation is raised to about 28 % due to weaker confinement. Besides, the D_r of this process is faster compared with TMV within TPEG gel where the mesh size is smaller, suggesting the potential effect of the term $\frac{\xi}{d}$, which we have introduced in Eq. (3), on the rotation process. The TMSD of the TMV-TPEG system exhibits a plateau-like regime at a long time scale (Supplementary Fig. 7), which is consistent with the fitting analysis. The ratio of the characteristic rotation re-orientation mode is only 10%, and its contribution to the translational diffusion is limited. On the other hand, both the TMSD and data fitting of the TMV-PEGDA system are similar to that of the NR85-PEG system. The diffusion of TMV in the PEGDA matrix is even faster than NR85 in the PEG matrix at a long time scale, which may have originated from the effect of large mesh size.

The extension to the biological system not only proves the universality of our method and theory but also indicates the existence of the typical range for the application of the dynamics model. With the increasing of the ratio $\frac{L}{\xi}$, the ratio of the characteristic rotation re-orientation process decreases. There should be a critical value of $\frac{L}{\xi}$ above which the proposed dynamics model doesn't hold, as the physical picture of the system will transform to rod reptation, and this value should be close to $\frac{L}{\xi} \sim 15$, as suggested by our experiments of the TMV-TPEG system.

Discussion

In summary, we have combined theoretical analysis, DLS, and DDLS experiments to investigate the dynamics of nanorods under confinement. The rotation process is highly coupled to the translational diffusion of nanorods. Our experiments demonstrate that the faster translation of the rod compared to the sphere within the networks originates from the characteristic rotation re-orientation process of the rod, and this process can be extended to biological systems, e.g., rod-like TMV, projecting the applications of our discovery in biomedical engineering. As the key discovery, the combination of theoretical analysis and light scattering studies shows that this rotation behavior follows a stretched exponential decay with exponent $\beta = 0.25$, while the dependence of D_r on mesh size, rod length, and rod diameter is also verified via scaling argument. Our work provides direct evidence for the rotation-facilitated translation of nanorods under nanoconfinement. The conclusions provide feasible approaches to tune the rotation and translation dynamics of synthetic or biological NPs confined in bio-tissues for practical applications.

Methods

Materials

The tetra-PEG macromers, tetra-PEG-amine (TPEG-A) 40 k, and tetra-PEG-succinimidyl glutarate (TPEG-S) 40k are purchased from JenKem. The PEGDA macromer is purchased from Peking PEG. Citric acid, dibasic sodium phosphate, sodium phosphate dibasic heptahydrate, and sodium phosphate monobasic dihydrate are purchased from Aladin. The gold nanoparticles NR50, NR85, NS32, and NS16 are purchased from LMnano, and these gold nanoparticles are grafted with CTAB (Hexadecyltrimethylammonium bromide). TMV is extracted from infected *Nicotiana cbenthamiana* leaves[42,43].

Sample preparation

TPEG-A and TPEG-S are dissolved in phosphate buffer (50 mM, pH 7.4) and phosphate-citrate buffer (50 mM, pH 5.8), respectively, by vortexing the solutions for 30 s. All studies are conducted at a TPEG concentration of 40 mg/mL. For samples loaded with nanoparticles, the nanoparticle solutions are directly added to the TPEG solution. All of the solutions are filtered using a membrane of 450 nm meshed. The filtered solutions are injected into the sample cell, and the solutions will become gel in 30 min. PEGDA is dissolved in water at a concentration of 25 mg/mL, the initiator 2959 was used to initiate the reaction under UV light, and the concentration of initiator is 2 mg/mL. The method loading of TMV within PEGDA hydrogel is the same as in TPEG system.

SAXS

The SAXS experiments were conducted at the BL10U1 beamline at the Shanghai Synchrotron Radiation Facility.

TEM

The TEM experiments were conducted at the JEM-1400 flash built by JEOL. The sample is prepared by soaking the holey carbon film on the copper grid in the solution sample for 1 s and dried in the air.

Rheology

Rheological investigations were performed at Anton Paar MCR302 rheometer.

Light scattering and the respective correction of non-ergodicity

The light scattering spectrometer used is a 3D-DLS Spectrometer (LS instruments, Switzerland), and the wavelength is 660 nm.

Dynamic light scattering (DLS) probes the dynamics of target objects at spatial scales of the q vector:

$$q = \frac{4\pi n}{\lambda}\sin\left(\frac{\theta}{2}\right) \tag{10}$$

Where n is the refractive index of the solvent, λ is the wavelength of the incident laser, and θ is the scattering angle[19]. The temporal window of dynamics measurements is limited by the sensitivity of the photon detector and the processing capability of digital correlators, and generally, the window is from 10 ns to 1 s, covering the typical rotation and translation dynamics of NPs and network fluctuation dynamics.

The formed tetra-PEG hydrogels and the hydrogels with NPs incorporated systems are nonergodic since the spatial constraints from the gel networks inhibit colloidal objects to decorrelate from their initial position. As a result, the time-averaged quantities could not be consistent with the properties of ensemble-averaged quantities. Pusey and co-workers developed a method to acquire the ensemble-averaged first-order correlation function $g_{1,E}(q,t)$ based on time-averaged correlation functions of a sub-ensemble[44]. The specific expression is shown below:

$$g_{1,E}(q,t) = 1 + \frac{1}{Y}\left[\sqrt{g_2(q,t) - \sigma_T^2} - 1\right] \tag{11}$$

where $Y = \langle I(q)\rangle_E / \langle I(q)\rangle_T$. $\langle I(q)\rangle_E$ is the ensemble-averaged scattering intensity measured from the time-averaged scattering intensity while rotating the sample (different sub-ensembles), and $\langle I(q)\rangle_T$ is the time-averaged scattered intensity measured similar to $\langle I(q)\rangle_E$ but keeping the sample at a fixed position. $g_2(q,t)$ is the second-order correlation function obtained from experiments. σ_T^2 is the mean-square intensity fluctuation ($\sigma_T^2 = \frac{\langle I^2(q)\rangle_T}{\langle I(q)\rangle_T^2} - 1$), which is the same as the intercept of $g_2(q,t) - 1$. The first-order correlation function can be divided into two parts, $g_{1,F}(q,t)$ (dynamic component) and $g_{1,s}(q)$ (static component), as follows:

$$g_{1,s}(q) = g_{1,E}(q,\infty) \tag{12}$$

$$g_{1,F}(q,t) = g_{1,E}(q,t) - g_{1,s}(q) \tag{13}$$

On the other hand, the DDLS technique is applied by integrating a polarizer in front of the photon detector, which is perpendicular (horizontal) to the polarization direction of the incident laser (vertical). Therefore, only the depolarized signal (VH) reaches the detector, and in our systems, only the dynamics information of nanorod samples is visible under DDLS mode since only anisotropic particles can change the polarization direction of the scattered light[35]. Both the translational and rotational processes contribute to the measured correlation function, and they are mixed as follows:

$$g_{1,VH}(q,t) = \exp(-q^2 W(t))\exp(-6\Omega(t)) \tag{14}$$

or

$$g_{1,E}(q,t) = \exp(-q^2 D_t t + 6D_r t) \tag{15}$$

where $W(t)$, $\Omega(t)$, D_t and D_r denote translational process, rotational process, and translational and rotational diffusion coefficients, respectively. Translational (TMSD, $\langle \delta r^2(t)\rangle$) and rotational mean-square (RMSD, $\left\langle \delta\theta^2(t)\right\rangle$) displacements can also be extracted as follows[20]:

$$\langle \delta r^2(t)\rangle = \frac{6}{q_2^2 - q_1^2}\ln\left|\frac{g_{1,E,VH}(q_1,t)}{g_{1,E,VH}(q_2,t)}\right| \tag{16}$$

$$\left\langle \delta\theta^2(t)\right\rangle = \frac{2}{3(q_2^2 - q_1^2)}\ln\left|\frac{g_{1,E,VH}(q_2,t)^{q_1^2}}{g_{1,E,VH}(q_1,t)^{q_2^2}}\right| \tag{17}$$

In short, DDLS can extract the dynamical processes and the comparison between DDLS and DLS is crucial to the attribution of hierarchical dynamics of particles confined in networks, especially for the identification of rotational processes.

Data fitting of the stretched exponential functions

Both of multiple modes fitting and CONTIN method are used to analyze the correlation function, where CONTIN is used to help the confirmation of the multiple modes. The correlation function after the non-ergodicity correction was fitted by a sum of exponential decays and stretched exponential decays in order to facilitate comparison to the theory proposed. The correlation function was fitted using ORIGIN software by minimizing the error between the fitted curve and the data, and Iterations were performed until the best-fitting curve was obtained. Besides, the residuals are randomly distributed about zero, and no systematic fluctuations in their mean can be observed.

Reporting summary

Further information on research design is available in the Nature Portfolio Reporting Summary linked to this article.

Data availability

All data that support the findings of this work are available within the paper and the Supplementary Information files. All data are available from the corresponding author upon request.

References

1. Chauhan, V. P. et al. Fluorescent nanorods and nanospheres for real-time in vivo probing of nanoparticle shape-dependent tumor penetration. *Angew. Chem. Int. Ed.* **50**, 11417–11420 (2011).
2. Bao, W. E. et al. Experimental and theoretical explorations of nanocarriers' multistep delivery performance for rational design and anticancer prediction. *Sci. Adv.* **7**, https://doi.org/10.1126/sciadv.aba2458 (2021).
3. Yu, X., Li, Y., Wu, J. & Ju, H. Motor-based autonomous microsensor for motion and counting immunoassay of cancer biomarker. *Anal. Chem.* **86**, 4501–4507 (2014).
4. Hansen-Bruhn, M. et al. Active intracellular delivery of a Cas9/sgRNA complex using ultrasound-propelled nanomotors. *Angew. Chem. Int. Ed.* **57**, 2657–2661 (2018).
5. Ge, T. Scaling perspective on dynamics of nanoparticles in polymers: length- and time-scale dependent nanoparticle–polymer coupling. *Macromolecules* **56**, 3809–3837 (2023).
6. Zhao, B. R., Li, B. & Shi, X. Molecular simulation of the diffusion mechanism of nanorods in cross-linked networks. *Nanoscale* **13**, 17404–17416 (2021).
7. Yu, M. et al. Rotation-facilitated rapid transport of nanorods in mucosal tissues. *Nano Lett.* **16**, 7176–7182 (2016).
8. Rose, K. A. et al. Shape anisotropy enhances nanoparticle dynamics in nearly homogeneous hydrogels. *Macromolecules* **55**, 8514–8523 (2022).
9. Yu, M. et al. Rapid transport of deformation-tuned nanoparticles across biological hydrogels and cellular barriers. *Nat. Commun.* **9**, 2607 (2018).
10. Fakhri, N., MacKintosh, F. C., Lounis, B., Cognet, L. & Pasquali, M. Brownian motion of stiff filaments in a crowded environment. *Science* **330**, 1804–1807 (2010).
11. Choi, J. et al. Fast nanorod diffusion through entangled polymer melts. *ACS Macro Lett.* **4**, 952–956 (2015).
12. Zhang, X. et al. Dynamic heterogeneities of rod rotation in macromolecular networks. *Macromolecules* **56**, 8428–8437 (2023).
13. Zhang, X. et al. Unconventionally fast transport through sliding dynamics of rodlike particles in macromolecular networks. *Nat. Commun.* **15**, 525 (2024).
14. Smith, M., Poling-Skutvik, R., Slim, A. H., Willson, R. C. & Conrad, J. C. Dynamics of flexible viruses in polymer solutions. *Macromolecules* **54**, 4557–4563 (2021).
15. Jia, D. & Muthukumar, M. Electrostatically driven topological freezing of polymer diffusion at intermediate confinements. *Phys. Rev. Lett.* **126**, 057802 (2021).
16. Reiser, M. et al. Photo-controlled dynamics and transport in entangled wormlike micellar nanocomposites studied by XPCS. *Macromolecules* **55**, 8757–8765 (2022).
17. Wu, H. et al. Spatial-temporal characteristics of confined polymer motion determine proton conduction of polyoxometalate-poly(ethylene glycol) hybrid nanocomposites. *J. Phys. Chem. Lett.* **9**, 5772–5777 (2018).
18. Bailey, E. J. & Winey, K. I. Dynamics of polymer segments, polymer chains, and nanoparticles in polymer nanocomposite melts: A review. *Prog. Polym. Sci.* **105**, 101242 (2020).
19. Berne, B. J., Pecora, R. *Dynamic Light Scattering: With Applications to Chemistry, Biology, and Physics*. Dover, New York (1976).
20. Gutiérrez-Sosa, C., Merino-González, A., Sánchez, R., Kozina, A. & Díaz-Leyva, P. Microscopic viscoelasticity of polymer solutions and gels observed from translation and rotation of anisotropic colloid probes. *Macromolecules* **51**, 9203–9212 (2018).
21. Balog, S. et al. Characterizing nanoparticles in complex biological media and physiological fluids with depolarized dynamic light scattering. *Nanoscale* **7**, 5991–5997 (2015).
22. Han, C. C. & Akcasu, A. Z. *Scattering and Dynamics of Polymers: Seeking Order in Disorderd Systems.* (John Wiley & Sons, 2011).

23. Tsuji, Y., Li, X. & Shibayama, M. Evaluation of mesh size in model polymer networks consisting of tetra-arm and linear poly(ethylene glycol)s. *Gels* **4**, 50 (2018).
24. Morozova, S. & Muthukumar, M. Elasticity at swelling equilibrium of ultrasoft polyelectrolyte gels: comparisons of theory and experiments. *Macromolecules* **50**, 2456–2466 (2017).
25. Jia, D. & Muthukumar, M. Topologically frustrated dynamics of crowded charged macromolecules in charged hydrogels. *Nat. Commun.* **9**, 2248 (2018).
26. Kureha, T., Hayashi, K., Ohira, M., Li, X. & Shibayama, M. Dynamic fluctuations of thermoresponsive poly(oligo-ethylene glycol methyl ether methacrylate)-based hydrogels investigated by dynamic light scattering. *Macromolecules* **51**, 8932–8939 (2018).
27. Li, X., Nakagawa, S., Tsuji, Y., Watanabe, N. & Shibayama, M. Polymer gel with a flexible and highly ordered three-dimensional network synthesized via bond percolation. *Sci. Adv.* **5**, https://doi.org/10.1126/sciadv.aax8647 (2019).
28. Meroz, Y. & Sokolov, I. M. A toolbox for determining subdiffusive mechanisms. *Phys. Rep.* **573**, 1–29 (2015).
29. Ogijk, T. on the statistics and dynamics of confined or entangled stiff polymers. *Macromolecules* **16**, 1340–1344 (1983).
30. Rubinstein, M., Colby, R. H. *Polymer Physics*. Oxford University Press New York (2003).
31. Gennes, P.-g. D. *Scaling Concepts in Polymer Physics-Cornell University Pres*. Cornell University Press (1979).
32. de Gennes, P. G. Motions of one stiff molecule in an entangled polymer melt. *J. Phys.* **42**, 473–477 (1981).
33. de Gennes, P. G. Relaxation anomalies in linear polymer melts. *Macromolecules* **35**, 3785–3786 (2002).
34. Fernández, J. R., Juste, J. P., Liz-Marzán, L. M. & Lang, P. R. Dynamic Light Scattering of Short Au Rods with Low Aspect Ratios. *J. Phys. Chem. C* **111**, 5020–5025 (2007).
35. Balog, S. et al. Dynamic depolarized light scattering of small round plasmonic nanoparticles: When imperfection is only perfect. *J. Phys. Chem. C* **118**, 17968–17974 (2014).
36. Watanabe, N., Li, X. & Shibayama, M. Probe diffusion during Sol–Gel transition of a radical polymerization system using isorefractive dynamic light scattering. *Macromolecules* **50**, 9726–9733 (2017).
37. Wang, J., Hu, W. Roles of repeating-unit interactions in the stress relaxation process of bulk amorphous polymers: 2. nonlinear viscoelasticity. *Polymer* **260**, 125367 (2022).
38. Mason, T. G. & Weitz, D. A. Optical measurements of frequency-dependent linear viscoelastic moduli of complex fluids. *Phys. Rev. Lett.* **74**, 1250–1253 (1995).
39. Dasgupta, B. R., Tee, S. Y., Crocker, J. C., Frisken, B. J. & Weitz, D. A. Microrheology of polyethylene oxide using diffusing wave spectroscopy and single scattering. *Phys. Rev. E* **65**, 051505 (2002).
40. Molaei, M., Atefi, E. & Crocker, J. C. Nanoscale rheology and anisotropic diffusion using single gold nanorod probes. *Phys. Rev. Lett.* **120**, 118002 (2018).
41. Cush, R., Dorman, D. & Russo, P. S. Rotational and translational diffusion of tobacco mosaic virus in extended and globular polymer solutions. *Macromolecules* **37**, 9577–9584 (2004).
42. Xie, G. et al. Conjugating peptides onto 1D rodlike bionanoparticles for enhanced activity against gram-negative bacteria. *Nano Lett.* **21**, 1722–1728 (2021).
43. Bruckman, M. A. & Steinmetz, N. F. Chemical Modification of the Inner and Outer Surfaces of Tobacco Mosaic Virus (TMV). In: *Virus Hybrids as Nanomaterials: Methods and Protocols* (eds Lin B., Ratna B.). Humana Press (2014).
44. Pusey, P. N. & Van Megan, W. Dynamic light scattering by non-ergodic media. *Phys. A* **157**, 705–741 (1989).

Acknowledgements

We would like to thank the support from BL16B1, BL19U2, and BL10U1 of Shanghai Synchrotron Radiation Facility for the access to the synchrotron-based SAXS. The helpful discussion with Prof. Litang Yan is acknowledged. Y.T. thanks the National Natural Science Foundation of China (31971303 and 52273160) for financial support. P.Y. acknowledges the financial support from the National Natural Science Foundation of China (Nos. 22241501 and 92261117), the Guangdong-Hong Kong-Macao Joint Laboratory for Neutron Scattering Science and Technology, the Open Fund of the China Spallation Neutron Source Songshan Lake Science City (DG24313519) and TCL science and technology innovation fund (No. 20222056).

Author contributions

P. C. Y. designed the research; B. H. X. and Y. L. prepared samples and performed research; Y. T. prepared TMV samples; B. H. X. analyzed data, and B. H. X. and P. C. Y. wrote the paper.

Competing interests

The authors declare no competing interests.

Additional information

Supplementary information The online version contains supplementary material available at https://doi.org/10.1038/s41467-024-50859-z.

Correspondence and requests for materials should be addressed to Panchao Yin.

Peer review information *Nature Communications* thanks the anonymous reviewers for their contribution to the peer review of this work. A peer review file is available.